



Subject: STTR PHASE I FINAL REPORT  
Author: Norman Laman, Thomas Tongue  
STTR Topic #: AF08-009  
Contract #: FA9550-09-C-0059

Date: 8/26/09  
Submission Date: 8/26/09  
Page: 1 of 21

---

## **Intense and Broadband THz Source using Laser-Induced Gas Plasma**

### **Phase I Final Report**

**Report Period: 11/1/2008 – 7/31/2009**

**Contract: FA9550-09-C-0059**

**CLIN#: 0001CC**

**Prepared by**  
**Norman Laman, Thomas Tongue**  
**Zomega Terahertz Corporation**

**Jianming Dai, X.-C. Zhang**  
**Rensselaer Polytechnic Institute**

**Submitted: 8/26/2009**

**Contractor for this Project:**



**Zomega Terahertz Corporation**  
1223 Peoples Ave  
Troy, NY 12180  
T/518 833 0577 F/518 833 6718

<b>Report Documentation Page</b>			Form Approved OMB No. 0704-0188		
<p>Public reporting burden for the collection of information is estimated to average 1 hour per response, including the time for reviewing instructions, searching existing data sources, gathering and maintaining the data needed, and completing and reviewing the collection of information. Send comments regarding this burden estimate or any other aspect of this collection of information, including suggestions for reducing this burden, to Washington Headquarters Services, Directorate for Information Operations and Reports, 1215 Jefferson Davis Highway, Suite 1204, Arlington VA 22202-4302. Respondents should be aware that notwithstanding any other provision of law, no person shall be subject to a penalty for failing to comply with a collection of information if it does not display a currently valid OMB control number.</p>					
1. REPORT DATE <b>27 AUG 2009</b>	2. REPORT TYPE	3. DATES COVERED <b>00-11-2008 to 00-07-2009</b>			
4. TITLE AND SUBTITLE <b>Intense and Broadband THz Source using Laser-Induced Gas Plasma</b>			5a. CONTRACT NUMBER		
			5b. GRANT NUMBER		
			5c. PROGRAM ELEMENT NUMBER		
6. AUTHOR(S)			5d. PROJECT NUMBER		
			5e. TASK NUMBER		
			5f. WORK UNIT NUMBER		
7. PERFORMING ORGANIZATION NAME(S) AND ADDRESS(ES) <b>Zomega Terahertz Corporation, 1223 Peoples Ave, Troy, NY, 12180</b>			8. PERFORMING ORGANIZATION REPORT NUMBER		
9. SPONSORING/MONITORING AGENCY NAME(S) AND ADDRESS(ES)			10. SPONSOR/MONITOR'S ACRONYM(S)		
			11. SPONSOR/MONITOR'S REPORT NUMBER(S)		
12. DISTRIBUTION/AVAILABILITY STATEMENT <b>Approved for public release; distribution unlimited</b>					
13. SUPPLEMENTARY NOTES					
14. ABSTRACT					
15. SUBJECT TERMS					
16. SECURITY CLASSIFICATION OF: a. REPORT      b. ABSTRACT      c. THIS PAGE <b>unclassified</b> <b>unclassified</b> <b>unclassified</b>			17. LIMITATION OF ABSTRACT <b>Same as Report (SAR)</b>	18. NUMBER OF PAGES <b>21</b>	19a. NAME OF RESPONSIBLE PERSON



## Executive Summary

The objective of the Phase I project was to create a compact, intense, broadband pulsed terahertz source suitable for use in a time domain spectroscopy system. This new source will cover a spectral range from 0.1 to 20 THz with an average power of 10 mW. In addition, we proposed to demonstrate spectroscopic measurements of explosives and related compounds.

During the period of the phase I project, the following major achievements were obtained:

- An in-line phase compensator was specifically designed, assembled and implemented in the THz air source. The specification of the in-line phase compensator is listed in Table I;
- More than 10 gases were tested. We demonstrated that certain organic gases have the potential for higher THz emission efficiency (refer to the pump-power dependent THz emission in different gases);
- THz electric field was further optimized with the in-line phase compensator, and a peak THz electric field of over 100 kV/cm is achieved, using excitation laser pulse energy less than 600  $\mu$ J. Stability of the system is improved from a few minutes previously to over 5 hours, with fine optical phase control better than a few atto-seconds.
- Incorporated with broadband THz-ABCD (THz-Air-Biased-Coherent-Detection) technique, we obtained a spectral bandwidth from 0.1 to about 25 THz (refer to Figure 18);
- We found the polarization of THz waves emitted from two-color laser-induced gas plasma can be coherently controlled by the relative phase between the two optical beams (800 and 400 nm beams)(Phys. Rev. Lett. 103, 023001 (2009)). This new finding will enable broadband modulation of intense THz waves using optical method, which was previously considered impossible;
- We also found the THz emission spectrum from laser-induced gas plasma changes as the relative phase between two optical beams changes—Phase dependent THz emission spectrum;
- Spectroscopic measurements of some explosives and their related compounds were performed with this new THz source in combination with THz-ABCD. Results are indicated in Figure 19;
- Finally, some papers related to this project were published or submitted during the phase I period—see Publications related to the project.

All the goals and criteria proposed in the phase I proposal have been met. Some achievements are already beyond what have been proposed, such as an improved spectral range over 25 THz (20 THz proposed), the discovery of the THz polarization effect versus relative optical phase, as well as phase-dependent THz wave emission spectrum. Future work in Phase II will include:

- Integration of Phase Compensator, Emitter and THz ABCD technique into single compact unit for stand-off explosive detection and NDT imaging.
- Increase the SNR of the system by at least 2 orders.
- Increase peak THz electric field above 1MV/cm for nonlinear THz spectroscopic applications
- Field test of this system for both close-distance and standoff sensing and identification of hazard materials, such as explosives.



## 1 Overview

This report will cover work that was completed during Phase I of contract FA9550-09-C-0059: "Intense and Broadband THz Source using Laser-Induced Gas Plasma", and disclose any inventions or computer programs that have been originated during the performance period. Any questions, comments or concerns regarding this report or the project should be sent to Zomega Terahertz Corporations technical point of contact:

Norman Laman  
Zomega Terahertz Corporation  
1223 Peoples Ave  
Troy, NY 12180  
Phone: (518) 833 0577  
E-mail: [nlaman@zomega-terahertz.com](mailto:nlaman@zomega-terahertz.com)

## 2 Background

Generation of intense THz radiation in the air has been demonstrated in three different THz wave generation configurations. Figure 1 schematically illustrates different geometries for generating THz waves by focusing optical beam(s) in air. The first approach is to focus a pulsed laser beam of 800 nm or 400 nm wavelength and 100 fs pulse duration into the air to create the plasma for THz wave radiation, as shown in Figure 1(a). The second approach is to place a barium-borate (BBO) crystal after the focal lens, shown in Figure 1(b). The third one, shown in Figure 1(c), combines the 800 nm & 400 nm beams (fundamental & its second-harmonic) by a dichroic mirror to provide coherent control of THz wave radiation through constructive or destructive interference between the two beams. For the purposes of this Phase I study, we rely on the complete control of the fundamental and second harmonic beams shown in Figure 1 (c) since the THz waves generated are orders of magnitude stronger than those from the system of Figure 1(a).

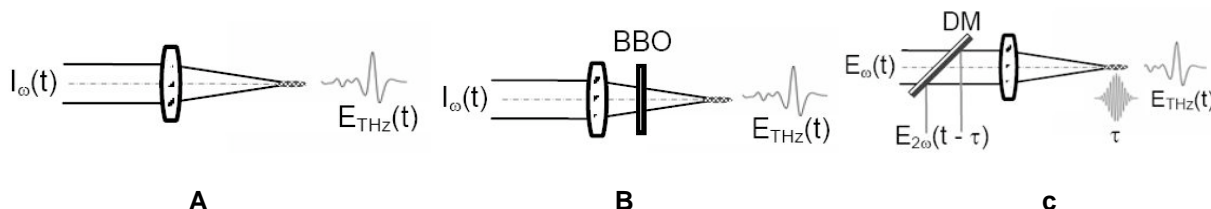


Figure 1: Schematic illustration of the three experimental setups: a. A pulsed optical beam ( $\omega$  or  $2\omega$ ) generates air plasma at the focal point; this optically-ionized plasma filament radiates a broadband THz wave, in which the THz wave generation is assigned to the ponderomotive force driving the electrons and ions. b. Introducing a nonlinear optical crystal (such as a 100  $\mu\text{m}$  thick type-I beta BBO crystal) after the lens generates the second-harmonic wave co-propagating with the fundamental, which are mixed in a third-order nonlinear optical process to create intense THz waves. c. A dichroic mirror combines the second-harmonic beam with the fundamental beam. Phase, amplitude and polarization of both beams can be controlled individually. When the fundamental optical beam is mixed with the second-harmonic beam, very strong THz wave radiation is observed by nonlinear optical frequency mixing in the air plasma. The THz wave polarity can be coherently controlled by changing the phase (through the time delay  $\tau$ ) between the two optical waves.

In the experimental arrangements in Figure 1(b) and (c), two beams (fundamental & its second-harmonic) are involved. Experimental results of Polarization and power dependence, with



independently controlled polarization and power of 800 nm and 400 nm, are consistent with Four-Wave-Rectification (FWR) theory<sup>1</sup> by the third-order polarization of the air plasma:

$$E_{\text{THz}}(t) \propto P^{(3)}(t) = \chi^{(3)} E_{2\omega}(t) E_\omega^*(t) E_\omega^*(t) \quad (1)$$

Where  $P$  is the dielectric polarization,  $\chi^{(3)}$  is the third-order nonlinear optical coefficient, and  $E$  is the electric field component associated with the optical field. Our experimental measurement shows that among many different possible combinations of the 800 nm, 400 nm and THz waves, the best possible configuration occurs when all the waves have the same polarization, i.e. P-polarization. Eqn. (1) can then be written as below:

$$E_{\text{THz}}(t) \propto \chi_{xxxx}^{(3)} E_{2\omega}(t) E_\omega^*(t) E_\omega^*(t) \cos(\varphi) \quad (2)$$

Where  $\varphi=2\omega\tau$  is the phase shift between the fundamental wave (800 nm) and the second-harmonic (400 nm),  $\tau$  is the corresponding time delay, as shown in Figure 1(c). The time delay  $\tau$  can be externally and precisely controlled, which is one of the core functions of our developed phase compensator discussed later in the report. From Eqn. (2), the THz field amplitude increases linearly with the energy of the 800 nm beam, and the square root of 400 nm energy. The exception is that at certain energy points the slope is changed dramatically. This point is very close to the tunnel ionization threshold in air. The identical subscripts in  $\chi_{xxxx}^{(3)}$  in Eqn. (2) indicates all the polarizations are in the same direction.

Figure 2(a) plots the measured peak THz field from a group of inert gases. As predicted in Eqn. (2), THz field is proportional to the third order nonlinearity ( $\chi^{(3)}$ ) in low gas pressure. Eqn. (2) also shows the phase  $\varphi$  between two optical beams. By adjusting the half-wave plates in the  $\omega$  and  $2\omega$  beam paths by as much as 0.67 fs ( $\Delta\varphi = \pi$ ), opposite polarizations of THz wave are measured, as shown in Figure 2(b).

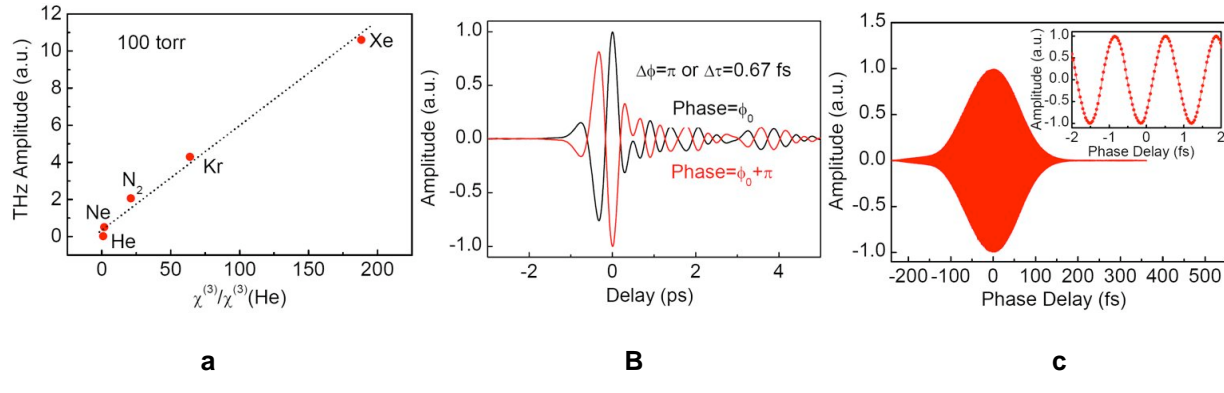


Figure 2(a) Peak THz field versus normalized  $\chi^3$ . Generated THz field is linearly proportional to the static  $\chi^3$ . (b) THz waveform flips when the phase difference between the  $\omega$  and  $2\omega$  beam is changed by  $\pi$ . This corresponds to about 667 attoseconds additional time-delay. (c) Temporal interference pattern of rectified field measured by monitoring THz pulse peak amplitude. Insert is the extended scale (4 fs) of the phase delay.

<sup>1</sup> Boyd, R. W., Nonlinear optics, Academic Press, Boston (1992).



Subject: STTR PHASE I FINAL REPORT  
Author: Norman Laman, Thomas Tongue  
STTR Topic #: AF08-009  
Contract #: FA9550-09-C-0059

Date: 8/26/09  
Submission Date: 8/26/09  
Page: 5 of 21

---

Figure 2(c) plots the temporal interference pattern of the rectified wave (THz field). When both the polarization of  $\omega$  and  $2\omega$  beams are parallel, the emitted THz wave has maximum amplitude in the same polarization which corresponds to  $\chi^{(3)}_{xxxx}$ . In general, the nonlinear effect from  $\chi^{(3)}$  is much weaker than that from  $\chi^{(2)}$  (commonly found in non-central symmetric crystals). However, due to material damage in solids by a high power laser, gases with large  $\chi^{(3)}$  are ideal candidates for the broadband and high field THz source.

There are three factors that limit the THz energy conversion efficiency using air-plasmas: (1) The polarizations, intensities, and phases of the fundamental beam and its second harmonic should be controlled independently to further optimize the emitted THz waves; (2) Ambient air (78% nitrogen) or nitrogen gas at atmospheric pressure does not guarantee the best THz conversion efficiency among the different gases; and (3) The limited pump energy (<mJ pulse energy from most amplified lasers).

In order to solve the above limitations, we designed a phase compensator, shown in Figure 3(a), to individually control the polarizations and intensities of the fundamental beam ( $\omega$ , 800 nm) and second harmonic ( $2\omega$ , 400 nm), and to precisely control the relative phase between the  $\omega$  and  $2\omega$  beams. The design of the phase compensator works well in a research lab, especially because it can independently control the amplitude, phase and polarization of both beams. However, these advantages are not necessary in the commercial product, and the current design limits the compactness of the THz-ABCD spectrometer. We propose a new phase compensator, shown in Figure 3(b), which is very compact (the size of a pen) and robust. We also estimate the average THz power will be increased by a factor of 4, in comparison to the old design in Figure 3(a).

The working principle of the "in-line" phase compensator shown in Figure 3(b), is as follows: The 800 nm fs pulse generates its second harmonic (2 $\omega$ , 400 nm) after passing through a BBO crystal. After passing through a bi-refringent plate (with  $\omega$  beam polarization aligned with the fast axis of the plate, and the  $2\omega$  beam with the slow axis) the  $\omega$  pulse propagates ahead of  $2\omega$  by a fixed time offset. The fast axis of the bi-refringent wedge pair aligns with the polarization of the  $2\omega$  beam, and the slow axis aligns with the polarization of the  $\omega$  beam. By changing the insertion, the relative phase shift when the two pulses reach the plasma spot can be continuously tuned across zero. A dual-band wave plate ( $\lambda/2$  retardance at 800 nm and  $\lambda$  at 400 nm) is used to rotate the polarization of  $\omega$  beam from S to P while keeping the polarization of  $2\omega$  pulse fixed, and consequently the polarizations of the two beams are the same. The detector in the figure can be a broadband THz-ABCD air sensor, EO crystal sensor, or Pyro-electric incoherent detector, depending on the application. Table 1 shows some specifications of the in-line phase compensator.

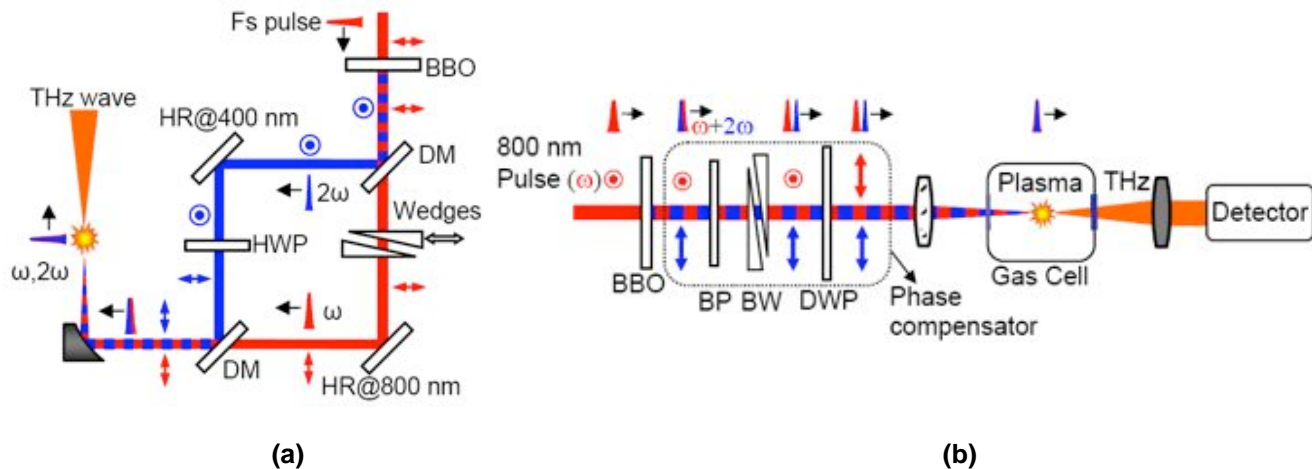


Figure 3(a) Schematic illustration of the phase compensator incorporated with a wedge pair: DM, dichroic mirror used to separate or re-combine the  $\omega$  and  $2\omega$  beam, HWP, half wave plate used to control the polarization of the  $2\omega$  beam; (b) The proposed phase compensator; The new design of the compact phase compensator is shown within the dotted line: BBO, type-I beta barium borate crystal; BP, bi-refringent parallel plate; BW, bi-refringent wedge pair; DWP, dual-band wave plate (half wave retardance at 800 nm and full wave retardance at 400 nm).

Table 1. Specifications of in-line phase compensator

Specification	Value	Comments
Phase Control Accuracy	< 3 attoseconds ( $< 1 \text{ nm}$ )	Phase control accuracy enables dynamic compensation and long term stability for system operation.
Phase Scanning Range	200 fs	$3.93^\circ$ wedge angle is used
Stability	< 0.5% Peak Power	Over a 6 hour period, less than 0.5% peak THz power change, primarily due to changes in the laser source itself.
Input Wavelength	800nm	
Input Power	$100\mu\text{J} - 6\text{mJ/pulse}$	
Output	400nm, 800nm	Output is collinear $\omega$ and $2\omega$ beam with parallel polarization.

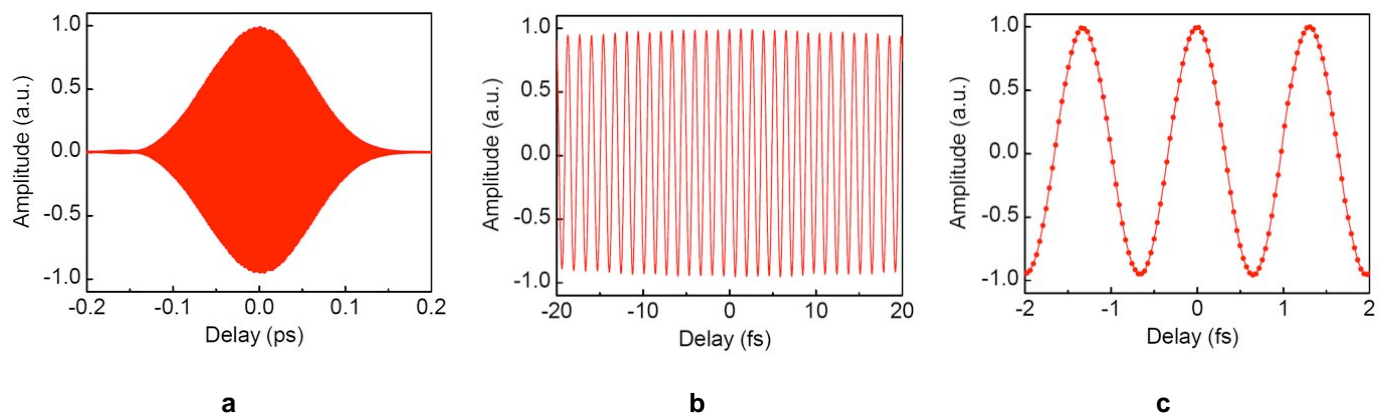


Figure 4(a) Measured peak THz signal versus time delay between  $\omega$  and  $2\omega$ ; (b) and (c) are subsets of the same data shown in expanded scale. Each delay step is 35 attoseconds; Measured THz field SNR > 1000:1 is achieved.

Figure 4(a) plots the measured peak THz signal versus time delay between  $\omega$  and  $2\omega$ ; Figure 4(b) and (c) are plots with expanded scale. The step of delay in Figure 4(c) is 35 attoseconds. Using a phase compensator to compensate the phase between  $\omega$  and  $2\omega$ , Our work performed in parallel with the Phase I effort demonstrated THz generation 116 meters away . The compensation concept works well, especially to reduce the perturbation by air turbulence in a long optical beam path. With this newly constructed phase compensator, the relative phase between 800 and 400 nm pulses can be precisely controlled within a sub-femtosecond which has far better stability than our requirement for standoff generation. Strong THz wave generation at standoff distances (>100 meters) has been demonstrated with the prototype phase compensator, by sending optical beams (800 nm and 400 nm) collinearly and creating plasma remotely. With the new design of the phase compensator, stable THz wave generation over 300 meters (even one kilometer) could be possible.

### 3 Experiments & Results

Below is a summary of activities completed during the Phase I study.



### 3.1 Evaluation of integrated phase compensator and gas cell THz source using pyroelectric detector

THz emission efficiency from gas plasma is directly related to the properties of these gases. Our initial experimental results with a gas jet<sup>2</sup> show that the THz emission efficiency of a certain gas is dominated by its 3<sup>rd</sup> order nonlinear susceptibility  $\chi^{(3)}$  if other factors, such as intensity clamping effect, dispersion of the gas, second-order nonlinear index of refraction, are negligible. However, in the real word applications, such a gas jet is not applicable.

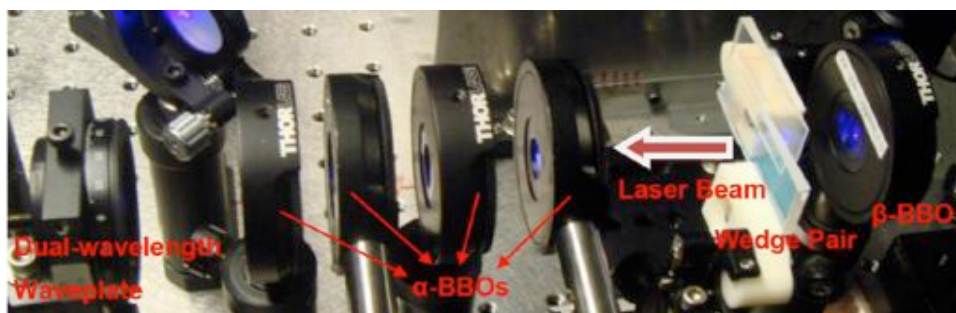
In this investigation, we performed some experiments with a gas cell incorporated with an in-line phase compensator on the THz emission efficiency using different gases as the THz wave emitter at 1 atm pressure. Experimentally, a pyroelectric detector rather than an electric-optic (EO) crystal is used for THz power detection due to the following purposes:

1. To minimize the polarization effect (EO sampling is polarization-sensitive);
2. To detect the THz signal in the full THz spectral range;
3. To minimize the effect that the THz beam size at the EO sensor may change when the plasma shapes are different for different gases (including the plasma length change);

#### 3.1.1 Experimental Setup

Figure 5(a) shows a photo of the phase compensator. The phase compensator is used to: (1) compensate the dispersion of the optical window of the gas cell; (2) compensate the dispersion in ambient air and the gas under test; (3) compensate the initial temporal walk-off between 800 nm ( $\omega$ ) and 400 nm ( $2\omega$ ) pulses right after the  $\beta$ -BBO for frequency doubling. Figure 5(b) shows a picture of the gas cell, which includes a 3-mm thick quartz window with both sides coated with an anti-reflection coating for wavelengths of 800 and 400 nm. A 3-mm thick high-resistivity float-zone silicon window is used for the transmission of the emitted THz wave. A parabolic mirror with an effective focal length of 150 mm is used to focus the  $\omega$  and  $2\omega$  optical beam to create a plasma. Using a regular mechanical vacuum pump, the gas pressure inside the gas cell can be pumped down to 1 mtorr, which is sufficient for the test.

(a)



<sup>2</sup> N. Karpowicz and X.-C. Zhang, Phys. Rev. Lett. 102, 093001 (2009).



(b)

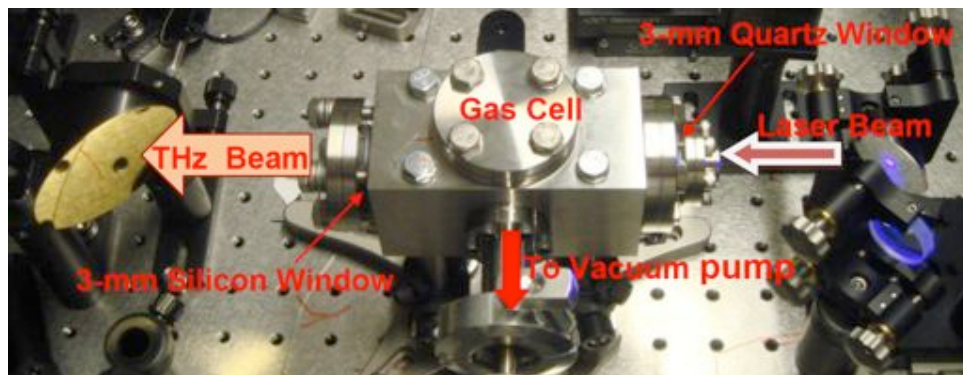


Figure 5: (a) A photo of the in-line phase compensator; (b) A photo of the gas cell used in the experiment.

To test the performance of the entire system, the THz signal with the gas cell evacuated or filled with ambient air (humidity=45%) was measured using EO sampling for higher sensitivity as shown in Figure 6. The ratio between the THz peak amplitudes with and without ambient air in the cell is about 1/300 in terms of THz electric field. So the ratio would be about 1/90,000 in terms of THz power. Since the dynamic range of the pyroelectric detector is less than 10000, the tiny THz signal with the gas cell evacuated cannot be detected with the power detector.

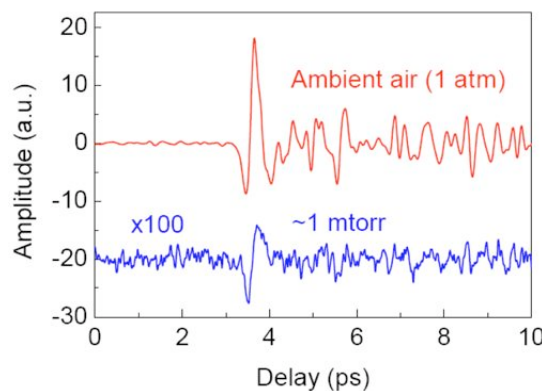


Figure 6: THz signals (waveforms) generated with the cell evacuated (in blue) and with the gas cell filled with ambient air at 1 atm (in red). The ratio in terms of amplitude is about 1/300.

### 3.1.2 Experimental Results

For each type of gas at 1 atm, a phase curve is obtained by scanning the relative phase between  $\omega$  and  $2\omega$  pulses through the translation of one of the wedges while monitoring the THz average power with the pyroelectric detector. The peak value of each phase curve stands for the THz emission efficiency for the corresponding gas type. Figure 7 shows the phase curves obtained with different gases. For the purpose of clarity, these curves are displayed in three different ways, as shown in Figure 7(a), (b), and (c), respectively.

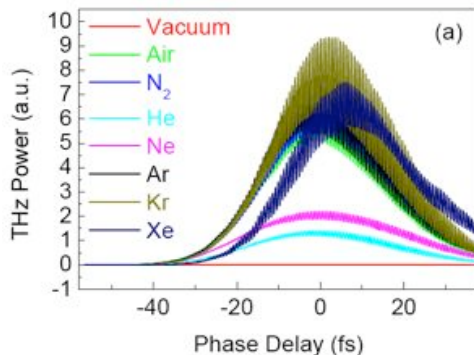


Figure 7(a) Original phase curves obtained with different gases.

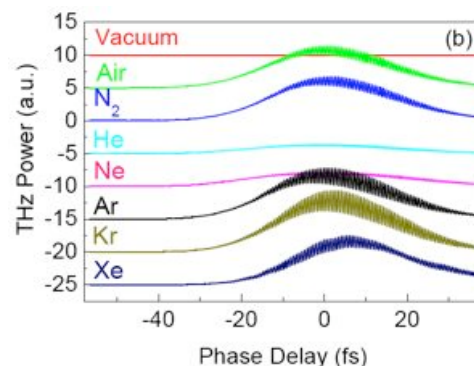


Figure 7(b). Phase curves obtained with different gases with their base line shifted vertically for clarity.

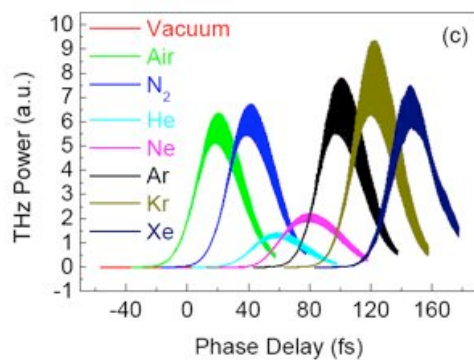


Figure 7(c). Phase curves obtained with different gases, shifted horizontally for clarity.

Table 22 indicates the relative THz emission efficiency with different gases as the THz wave emitter. The relative 3<sup>rd</sup> order nonlinear susceptibility ( $\chi^{(3)}$ ) of each gas is also listed for comparison. These results show that, the highest nonlinear susceptibility doesn't guarantee the highest THz emission efficiency, which varies substantially from the previous results with a gas jet where intensity clamping effect, dispersion of the gas, second-order nonlinear index of refraction are negligible.

Table 2: THz emission efficiency with different gases

Gas	$\chi^{(3)} / \chi^{(3)}_{(N_2)}$	THz emission efficiency (Compared to N <sub>2</sub> )
He	0.047	0.21
Ne	0.085	0.33
N <sub>2</sub>	1.0	1.00
Air (RH=45%)	~1.0	0.94



Ar	1.1	1.16
Kr	3.0	1.39
Xe	7.5	1.11
CH <sub>4</sub>	2.8	1.07
C <sub>2</sub> H <sub>6</sub>	5.1	0.80
C <sub>3</sub> H <sub>8</sub>	8.6	0.62
C <sub>4</sub> H <sub>10</sub>	11.1	0.45—(very unstable)

In order to confirm the lower THz emission efficiency from some gases with higher  $\chi^{(3)}$ , such as Xe and C<sub>4</sub>H<sub>10</sub>, is not due to the saturation effect or the intensity clamping effect, the pump-power dependent THz emission was tested for these two gases. Figure 8(a) and (b) show the pump-power dependences of THz emission with Xe and C<sub>4</sub>H<sub>10</sub>, respectively. Both the experimental curves indicate that they are still quite far from being saturated in the current experimental geometry using a parabolic mirror with 150 mm focal length (corresponding to a geometrical focal spot of about 40 microns).

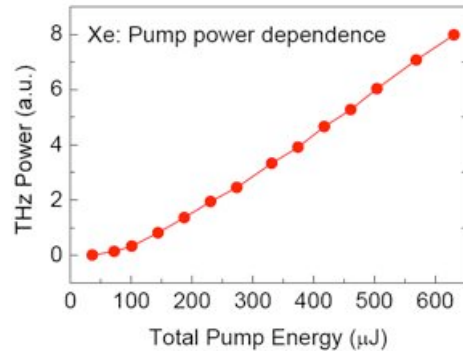


Figure 8(a): Emitted THz power versus optical pump power, using Xe gas as the THz wave emitter at 1 atm.

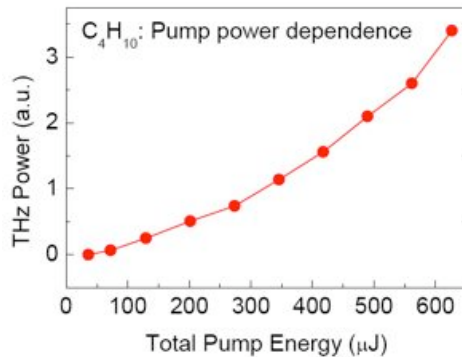


Figure 8(b): Emitted THz power versus optical pump power, using C<sub>4</sub>H<sub>10</sub> gas as the THz wave emitter at 1 atm.

One more important result is that, although C<sub>4</sub>H<sub>10</sub> has the highest  $\chi^{(3)}$ , its THz emission efficiency is not the highest. Even worse, the THz emission output of the C<sub>4</sub>H<sub>10</sub> based emitter is very unstable. Shown



in Figure 9 is the phase curve (in red) using  $C_4H_{10}$  gas as the emitter. For stability comparison, a typical phase curve from another gas (here we use  $C_3H_8$ ) is also printed in the figure.

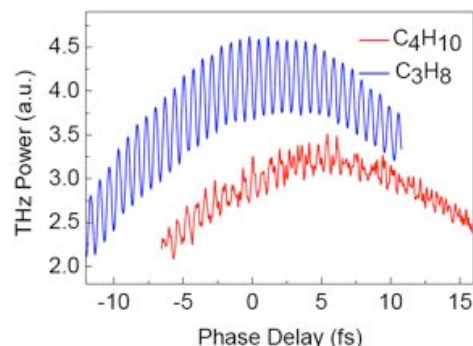


Figure 9: Phase curves for two different gases for THz signal stability comparison. The red curve is with  $C_4H_{10}$  gas, and blue curve is with  $C_3H_8$  gas.

### 3.2 Investigation of Phase Dependent THz Wave Polarization

To further optimize the THz emission efficiency with the in-line phase compensator, which is one of the most important objectives of the AF STTR project, we changed the polarization of the  $\omega$  (800 nm) and  $2\omega$  (400 nm) beams by tuning the dual-band waveplate, and then checked the emitted THz power with a pyroelectric detector while changing the relative phase between two optical beams. Figure 10 shows that elliptically polarized optical beams give rise to even higher THz emission from gas plasma than that when the  $\omega$  and  $2\omega$  beams are both linearly polarized and parallel to each other. However, when THz polarization-sensitive electric-optic sampling is used to detect electric field of the emitted coherent THz waves, the detectable peak THz electric field doesn't increase. In our specific experiments, there are two possible reasons why the detectable peak THz electric field doesn't increase when the average power of the emitted THz waves is doubled or even tripled: (1) Incoherent THz radiation occupies a large percentage in the total THz emission; (2) THz polarization is changed as the relative phase changes. Further experimental investigation was performed to check the incoherent (background) THz emission from plasma originated from the black body radiation or from the THz "fluorescence" similar to the spontaneous emission from excited laser media. Results show that, only less than 5% of the possible "incoherent THz emission" existing. This implies the undetectable increase in THz electric-field is the THz polarization effect.

In this report, we are going to introduce our new finding on the THz polarization change when the relative phase between the  $\omega$  and  $2\omega$  beams is changed<sup>3</sup>. Also we're going to report one more consequence induced by the relative phase change—the THz emission spectral characterization, which has not been published yet.

<sup>3</sup> J. Dai, N. Karpowicz, and X.-C. Zhang, "Coherent Polarization Control of Terahertz Waves Generated from Two-Color Laser-Induced Gas Plasma", *Phys. Rev. Lett.* **103**, 023001 (2009).

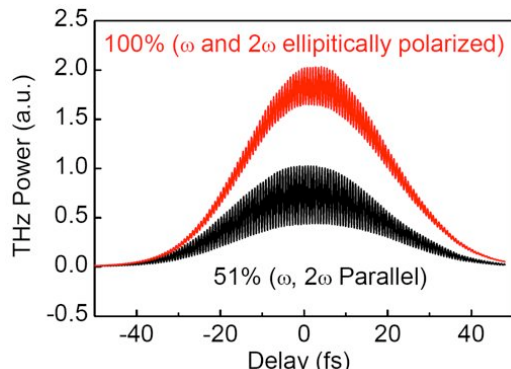


Figure 10: THz output power phase curves with elliptically polarized 800 and 400 nm beams and well-defined parallel polarized 800 and 400 nm beams.

### 3.2.1 Experimental Results

In order to systematically investigate the THz polarization effect in two-color laser-induced gas plasma. The in-line phase compensator as described in the previous report is incorporated, as shown in Figure 11. After a single color femtosecond pulse ( $\omega$ ) passes through the in-line phase compensator, the two pulses ( $\omega$  and  $2\omega$ ) are simultaneously focused into air or selected gases to create plasma and generate THz waves; the generated THz waves pass through a broadband THz polarizer and then are detected by a polarization-insensitive pyroelectric detector for power detection. The combination of the THz polarizer and the pyroelectric detector is actually used to inspect the polarization status of the emitted THz waves from gas plasma by monitoring the transmitted THz intensity (power) when the THz polarizer is rotating along the THz beam at each relative optical phase. Figure 12 is a typical phase curve obtained when the  $\omega$  and  $2\omega$  beams are both linearly polarized with their polarization directions parallel to each other by changing the relative phase between the  $\omega$  and  $2\omega$  pulses while monitoring at the emitted THz intensity (power) with the pyroelectric detector. Compared to the phase curves in Figure 10, this phase curve has much higher modulation depth with a minimal THz intensity of nearly "zero" at the central part of the curve. This is due to the well-defined polarizations of the  $\omega$  and  $2\omega$  beams.

When checking the emitted THz wave spectrum as the relative optical phase changes, instead of using the combination of the THz polarizer and the pyroelectric detector, we use a 0.3-mm thick GaP crystal through electric-optic sampling for coherent THz wave detection.

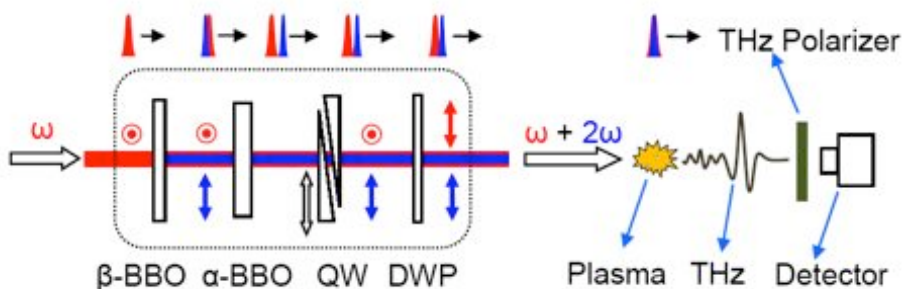


Figure 11: Schematic illustration of the experimental setup for the systematic investigation of the THz polarization effect. Inside the dashed line is the in-line phase compensator.  $\beta$ -BBO,



beta-barium borate crystal;  $\alpha$ -BBO, alpha-barium borate crystal; QW, quartz wedges; DWP, dual-wavelength waveplate; Detector, pyroelectric detector for THz power detection after the emitted THz waves pass through the THz polarizer; the red and blue arrows indicate the polarization of the  $\omega$  and  $2\omega$  beams, respectively.

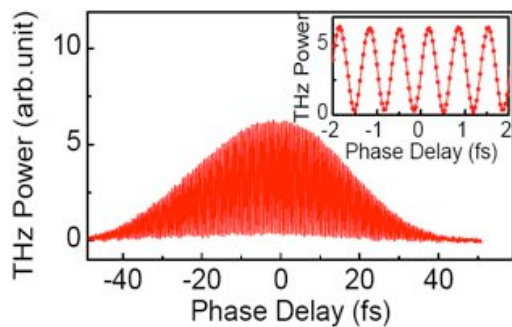


Figure 12: A typical phase curve obtained by changing relative phase between the  $\omega$  and  $2\omega$  pulses through the change of the insertion of one of the wedges while monitoring the THz average power with a pyroelectric detector when the  $\omega$  and  $2\omega$  pulses are linearly polarized and parallel to each other; the inset shows a zoomed-in portion of the phase curve.

### 3.2.2 Phase-dependent polarization of THz waves with linearly polarized optical pulses

Figure 13(a) and (b) show the change in measured THz intensity versus THz polarizer angle and the relative phase between  $\omega$  and  $2\omega$  pulses with the  $\omega$  and  $2\omega$  beams parallel and orthogonally polarized (the  $2\omega$  beam is kept vertically polarized), respectively. To indicate the THz polarization rotation more clearly, we present the same data in a 2D manner, as shown in Figure 13(c) and (d) for the cases when the  $\omega$  and  $2\omega$  beams parallel and orthogonally polarized, respectively. Obviously, Figure 13 indicates a higher THz emission efficiency when the  $\omega$  and  $2\omega$  pulses are parallel polarized, compared to the case when two optical pulses are orthogonally polarized. We also can see that, when both the  $\omega$  and  $2\omega$  pulses are linearly polarized, the polarization of the emitted THz waves (linearly polarized) is kept the same as the relative phase between the optical pulses changes, and that the THz polarization is basically follows the polarization of the  $2\omega$  pulse.

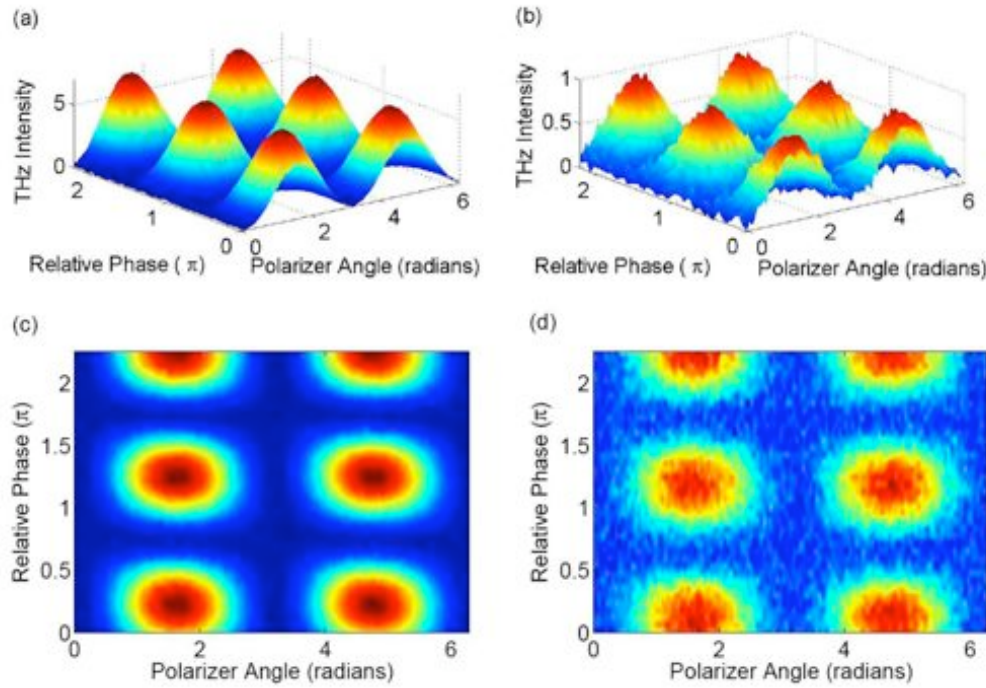


Figure 13: THz intensity versus THz polarizer angle and the relative phase between the  $\omega$  and  $2\omega$  pulses with linear polarization. (a) and (b) are experimental results with the two optical pulses parallel and orthogonally polarized, respectively; (c) and (d) represent the same data in a 2D manner with the  $\omega$  and  $2\omega$  pulses parallel and orthogonally polarized, respectively.

### 3.2.3 Phase-dependent polarization of THz waves with elliptically polarized optical pulses

When at least one of the  $\omega$  and  $2\omega$  pulses is elliptically or circularly polarized, we found the polarization direction of the emitted THz waves rotate as the relative optical phase changes. Figure 14 shows the experimental results on the THz polarization effect when the  $\omega$  pulse is left-handed or right-handed circularly polarized while the  $2\omega$  pulse is elliptically polarized with the ratio between the minor axis and major axis of the ellipse (defined here as ellipticity) of about 1/11 in terms of THz intensity.

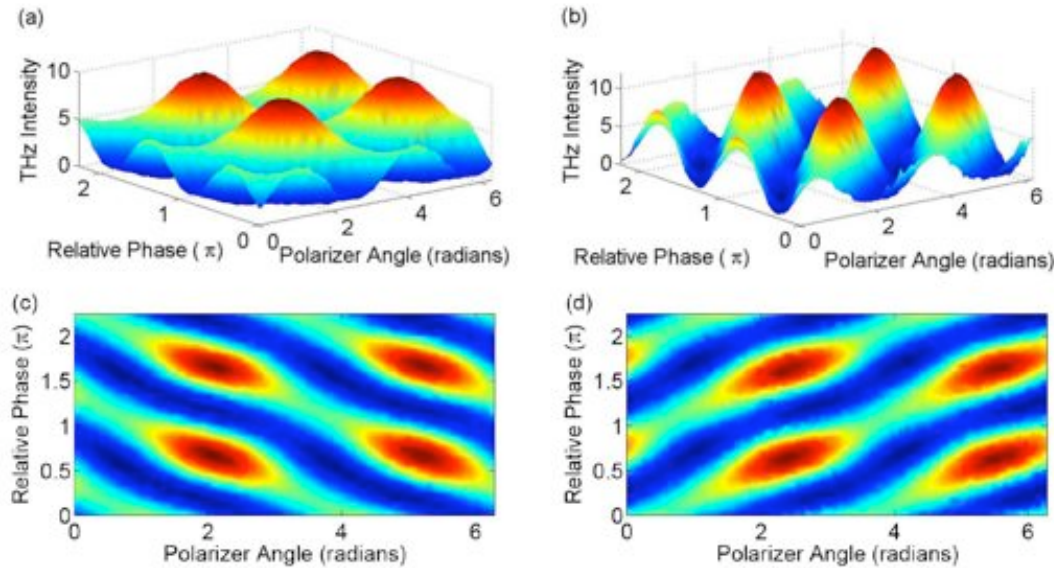


Figure 14: THz intensity versus THz polarizer angle and the relative phase between the  $\omega$  and  $2\omega$  pulses with circular or elliptical polarization. (a) and (b) when the  $\omega$  beam is left-handed and right-handed circularly polarized while the  $2\omega$  beam is elliptically polarized with the ratio between the minor axis and major axis of the ellipse (defined here as ellipticity) of about 1/11 in terms of THz intensity, respectively. (c) and (d) represent the same data in a 2D manner with the  $\omega$  pulse left-handed (corresponding to (a) in 3D manner) and right-handed circularly polarized (corresponding to (b) in 3D manner) while the  $2\omega$  pulse elliptically polarized, respectively. When the  $\omega$  beam is right-handed circularly polarized the THz polarization rotates in a right-handed manner, and vice versa.

More importantly, we found that, when both the  $\omega$  and  $2\omega$  beams are circularly-polarized the polarization of the emitted THz beam rotates while the intensity or the electric field of the THz wave is kept unchanged as the relative phase between the pulses changes, as shown in Figure 15. This particular situation is very important for some applications, such as THz modulation devices. Figure 15(a) and (b) show the experimental results when both  $\omega$  and  $2\omega$  beams are right-handed elliptically polarized with their ellipticities both higher than 0.8 (which means that both the  $\omega$  and  $2\omega$  beams are close to circular polarization).

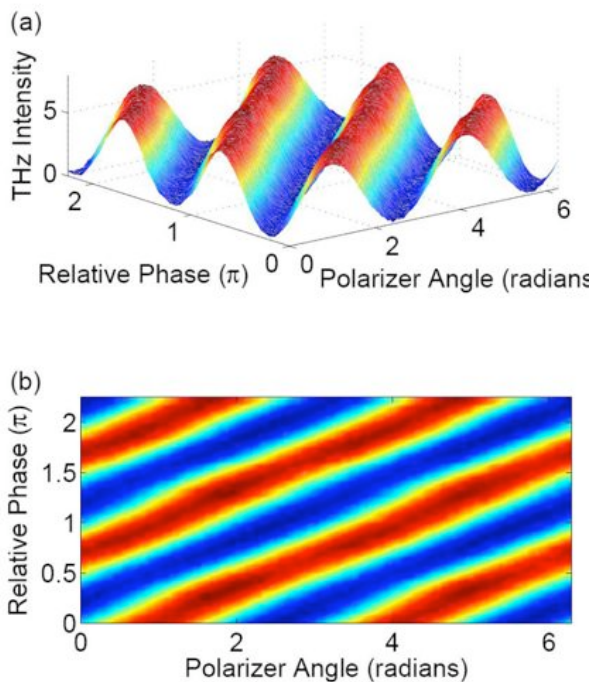


Figure 15: THz intensity versus THz polarizer angle and relative phase between  $\omega$  and  $2\omega$  pulses with both  $\omega$  and  $2\omega$  beams are right-handed circularly polarized. (a) Experimental data presented in a 3D manner, and (b) The same data presented in a 2D manner. Results indicate that, the THz polarization can be rotated by simply changing the relative phase between  $\omega$  and  $2\omega$  beams while keeping the amplitude of the THz wave constant.

Similar independent experimental results have also been reported by another group in Stanford University using different technical approach<sup>4</sup>, further verifying our observation in this report. All these experimental observation can be reproduced by the numerical simulation using the quantum mechanical model presented in our previous work<sup>2</sup>.

### 3.3 Phase-dependent THz emission spectrum in asymmetrically ionized gas plasma

Using a 0.3-mm GaP crystal, instead of a pyroelectric detector in Figure 11, we are able to detect the THz emission spectra at the relative phase. Figure 16 shows the THz waveforms at different relative optical phase values between the  $\omega$  and  $2\omega$  beams obtained through electric-optic sampling with the above GaP crystal.

<sup>4</sup> H. Wen, and A. Lindenberg, "Coherent Terahertz Polarization Control through Manipulation of Electron Trajectories", *Phys. Rev. Lett.* 103, 023902 (2009).

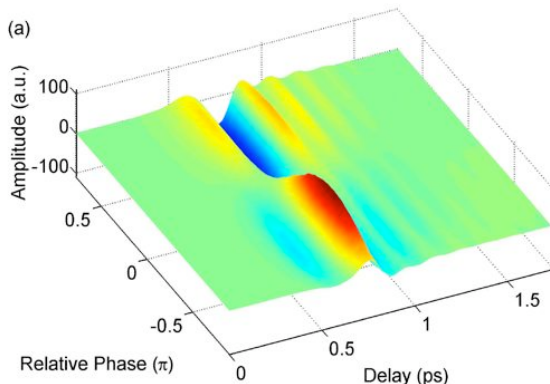


Figure 16: THz waveforms at different relative optical phases between the  $\omega$  and  $2\omega$  beams when  $\omega$  and  $2\omega$  beams are linearly polarized and parallel to each other.

Figure 17 shows the overall spectral change versus the relative phase between the  $\omega$  and  $2\omega$  beams in 3D plot through the discrete Fourier Transform of the waveforms shown in Figure 16. Figure 17(b) shows the normalized spectra when the  $\omega$  and  $2\omega$  beams are linearly polarized and parallel to each other. And Figure 17(c) shows some individual spectra near the relative optical phase value (here we refer to the value close to "zero") at which the emitted THz radiation is extremely weak. It is noteworthy that, the phase "zero" doesn't mean the absolute zero phase. In the current experiment, we are unable to measure the absolute phase.

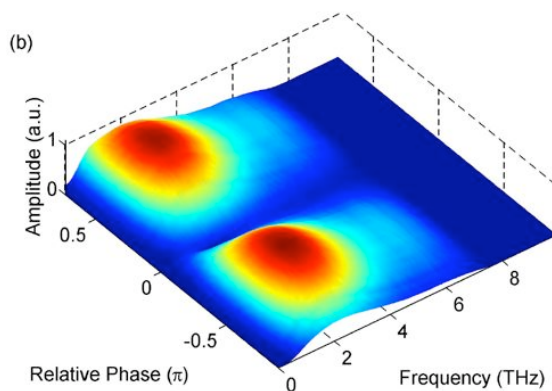


Figure 17(a): THz emission spectra at different relative optical phases in 3D plot when the  $\omega$  and  $2\omega$  beams are linearly polarized and parallel to each other.

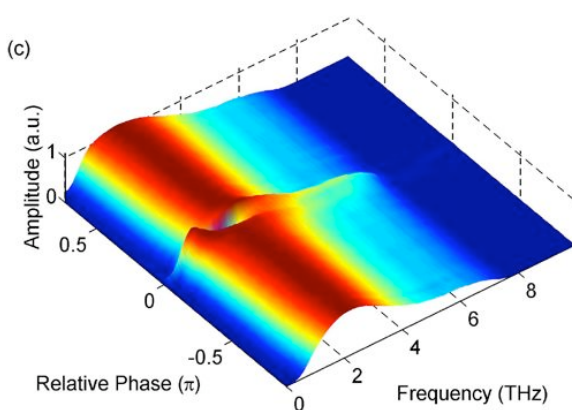


Figure 17(b): Normalized THz emission spectra at different relative optical phases in 3D plot.

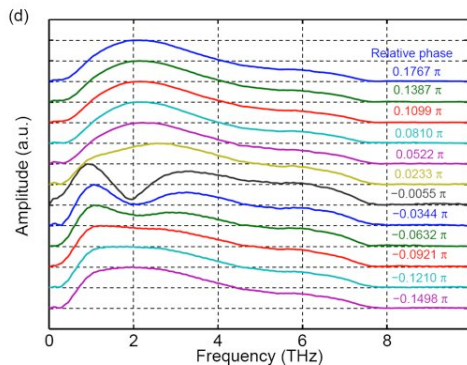


Figure 17(c): Normalized THz emission spectra at different relative phases near "zero". The spectra are shifted for clarity.

From Figure 16 and Figure 17(a)-(c), we can see that, the THz emission spectrum doesn't change too much before the relative optical phase approaches the values at which the emitted THz radiation is extremely weak. This result is very important for some applications such as THz remote sensing and identification, in which we hope the relative phase fluctuation won't significantly change the THz emission spectrum from femtosecond laser-induced gas plasma.

### 3.4 Spectral bandwidth of the system and spectroscopic measurements of some explosives and related compounds

Shown in Figure 18 are a typical THz waveform and the corresponding emission spectrum from the THz gas source incorporated with the in-line phase compensator. The spectrum is measured using THz-ABCD technique. From Figure 18 we can see a spectral coverage from 0.1 to 25 THz is achieved.

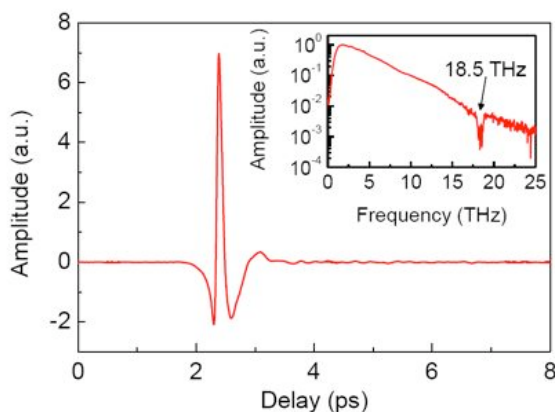


Figure 178: A typical THz waveform and its corresponding spectrum obtained with the new THz air source incorporated with an in-line phase compensator and the broadband THz-ABCD sensing technique. The main panel shows the THz waveform and the inset shows the corresponding spectrum. The dip around 18.5 THz as shown in the spectrum (inset) is due to the absorption from a high-resistivity silicon plate used to block the residual optical beams.



Spectroscopic measurements of some explosives and related compounds were also performed with the intense source in combination with THz-ABCD technique, as shown in Figure 19.

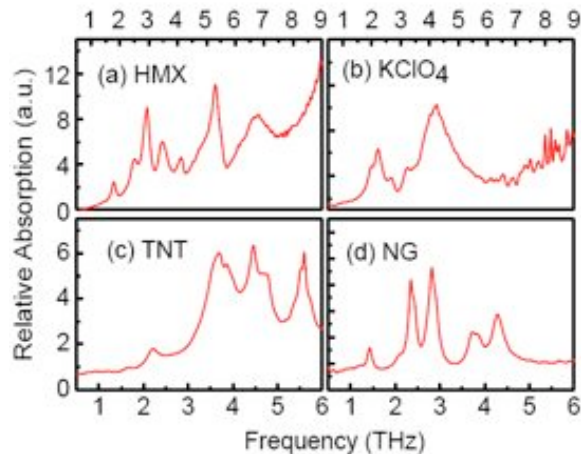


Figure 179: A Measured absorption spectra of four typical explosives with THz-ABCD spectrometer: (a) HMX, (b) KClO<sub>4</sub>, (c) TNT, and (d) NG (Nitroguanidine).

## 4 Inventions/Computer Programs Disclosure

No computer programs or inventions were developed during the reporting period.

## 5 Publications & Related Activities

Work performed during this STTR project had contributions to the following published and pending papers and conferences:

1. Jianming Dai, Thomas Tongue, X.-C. Zhang, "In-line phase compensator for intense THz generation in selected gases", *IRMMW-THz 2009, The 34rd International Conference on Infrared, Millimeter, and Terahertz Waves*, Paradise Hotel, Busan, Korea, September 21~25, 2009.
2. Jianming Dai, Nicholas Karpowicz, and X.-C. Zhang, "Optically manipulating terahertz wave polarization in two-color laser-induced gas plasma", *Optics & Photonics News (OPN)*, submitted (2009).
3. Jianming Dai, Nicholas Karpowicz, and X.-C. Zhang, "Coherent polarization control of terahertz waves generated from two-color laser-induced gas plasma", *Physical Review Letters* 103, 023001 (2009).
4. Jianming Dai and X.-C. Zhang, "Terahertz wave generation from gas plasma using a phase compensator with attosecond phase-control accuracy", *Applied Physics Letters* 94, 021117 (2009).
5. Nicholas Karpowicz and X.-C. Zhang, "Coherent terahertz echo of tunnel ionization in gases", *Physical Review Letters* 102, 093001 (2009).

In addition, Zomega has participated in several Department of Defense related activities which may enjoy benefits in the future from the Phase I and potential Phase II work:

- THz Characterization of Skin - Brooks Air Force Base (PI: Gerald Wilmink). This project has currently used the mini-Z THz Time Domain Spectrometer to measure the complex index of refraction of skin samples under a variety of conditions. Future work could benefit from the nonlinear spectroscopic capabilities of the air photonics approach as well as the enhanced spectral range (0.1 - 25 THz).



## 6 Final Comments

This Phase I project has resulted in the following conclusions:

- 1) Unlike our previous results with a gas jet, the highest nonlinear susceptibility doesn't guarantee the highest THz emission efficiency. In terms of real world applications, other nonlinear effects, such as intensity clamping effect, dispersion of the gas, second-order nonlinear index of refraction, have to be considered for the optimization of THz emission efficiency. The best THz emission efficiency using gases as the THz wave emitter is still far from being fully utilized;
- 2) From the pump power dependent results, we can conclude that, our current laser pump intensity with current experimental geometry is still quite far from the saturated intensity. Using a higher intensity lasers we can get much higher THz electric field (currently about 150 kV/cm). We also expect that, using TW femtosecond laser, by properly choosing the pump beam optical focal length, we can avoid the saturation effect and get even higher THz E-field;
- 3) THz wave emitted from C<sub>4</sub>H<sub>10</sub> gas is very unstable, indicating that this gas cannot be used as reliable THz emitter medium without further study;
- 4) THz polarization can be coherently controlled by changing the relative phase between the  $\omega$  and  $2\omega$  beams;
- 5) Theoretical simulation using a quantum mechanical model is performed, and is found to completely reproduce the new experimental observations (simulation results are not presented in this report—refer to reference<sup>2,4</sup>);
- 6) By knowing the above THz polarization effect, we further optimized the detectable THz field by properly changing the optical probe beam polarization to match the THz polarization. The detectable peak THz electric field is now over 100 kV/cm even using a total excitation laser energy less than 0.6 mJ;
- 7) The THz emission spectrum from femtosecond laser-induced gas plasma, and found that, the THz emission spectrum doesn't change significantly as the relative optical phase changes before the phase approaches a value at which a very weak THz emission is reached;
- 8) Possible applications of the THz polarization effect include fast, broadband modulation of intense THz waves without significant THz loss using an optical approach.